Dynamic drag of solute atmosphere on moving edge dislocations—Phase-field simulation

S. Y. Hu[a)]
Department of Materials Science and Engineering, The Pennsylvania State University, University Park, Pennsylvania 16802

J. Choi
Department of Metals and Materials Engineering, Kangnung National University, Korea

Y. L. Li and L. Q. Chen
Department of Materials Science and Engineering, The Pennsylvania State University, University Park, Pennsylvania 16802

(Received 25 February 2004; accepted 5 April 2004)

A solute atmosphere forms around a dislocation at temperatures where the diffusion of solute atoms is comparable to or faster than the dislocation motion. The dynamic interactions between diffusive solutes and moving dislocations were studied using a phase-field model which takes into account both the chemical interactions in the solid solution and the elastic interactions among solutes and dislocations. The average velocity of dislocations as a function of solute concentration, solute mobility, dislocation mobility, and applied stresses was investigated. The dragging stress of a solute atmosphere and the solute flow around a moving dislocation are presented and analyzed. Some features of dynamic interactions between a single dislocation and its solute atmosphere are observed. © *2004 American Institute of Physics.* [DOI: 10.1063/1.1755858]

I. INTRODUCTION

Solid solution hardening is a common phenomenon observed in many metallic alloy systems. It arises from various interactions between dislocations and solutes such as elastic interactions, chemical interactions, as well as electric interactions.[1–6] At low temperatures the diffusion of solute atoms is so slow that the solute atoms are almost at rest as dislocations move. As a result, the solutes act as point obstacles to moving dislocations. In this case, the elastic interactions between immobile solutes and moving dislocations have been studied. Statistic methods[7–9] were developed for estimating the critical resolved shear stress. Recently, a phase-field approach[10] was developed for studying the elastic interaction between randomly distributed immobile point obstacles and mobile dislocations in a two-dimensional model.

At moderate or elevated temperatures, however, solute diffusion becomes significant and a solute atmosphere forms quickly round moving dislocations.[11] The dynamic interaction between diffusing solute atoms and mobile dislocations causes a repeated yield-point phenomenon (serrated yielding) and an increase in yield strength with temperature, i.e., the Portevin–Le Chatelier effect, which has been observed in many alloys. There are a number of theoretical and experimental studies of the dynamic interactions between diffusing solute atoms and mobile dislocations.[12–16] For a single dislocation in two dimensions, the critical velocity for the formation of solute atmosphere, steady-state solute atmosphere and its dragging stress on a moving dislocation were analyzed by Cottrell and Jawon,[12] Lothe and Price Hirth[3] and Yoshinaga and Morozumi,[13] respectively. In these analyses, the chemical and elastic interactions among solute atoms were ignored and different degrees of simplification were made. Computer simulation of the Portevin–Le Chatelier effect were carried out using a simple spatial coupling model.[16] Kinetic Monte Carlo method[17] and molecular dynamic method[18] have also been employed for simulating the dynamic interactions between moving dislocations and diffusing solute atoms.

Recently, we proposed a continuum diffuse-interface field model[19,20] by coupling the Cahn–Hilliard diffusion equation[21] with the elastic fields produced from coherent compositional inhomogeneities as well as from structural defects such as dislocations. The unique feature of this model is that the structural defects are viewed as lattice distortions described by ''eigenstrain.'' It is capable of describing defects with an arbitrary spatial distribution. A recent advance in phase-field modeling of dislocation dynamics was made by Wang *et al.*[22–25] In their phase-field model, the dislocation loops are viewed as misfitting platelet inclusions, and labeled by a set of order parameter field variables. The temporal evolution of order parameter field variables, i.e., dislocation motion, is described by the phenomenological time-dependent Ginzburg–Landau kinetic equation.[26] It is shown that the model can take into account not only the long-range elastic interaction among dislocations, but also the short range interactions such as multiplication and annihilation of dislocations. Chen and Wang[27] generalized the crystalline energy and the gradient energy in previous phase field models[22] to account for dislocation reactions and simulated the formation of dislocation network. A similar phase-field model of dislocation dynamics was developed by Rodney *et al.*[28] In their model two length scales are employed to take into ac-

a)Electronic mail: sxh61@psu.edu

count the dislocation core size which is smaller than the grid space. However, it is computationally intensive, especially for a multidislocation system.

The phase-field model of dislocation dynamics in Ref. 22 has been extended into a binary alloy by incorporating diffusing solute atoms, immobile defects such inclusions, and elastic inhomogeneity.[29] The chemical and elastic interactions among solutes and dislocations are automatically taken into consideration. The focus of the present work is on modeling the dynamic dragging effect of the solute atmosphere on moving dislocations.

II. PHASE FIELD DESCRIPTION OF A BINARY SYSTEM WITH DISLOCATIONS

We consider a binary solid solution with a compositional inhomogeneity and a distribution of dislocations. Two sets of phase field variables, i.e., compositional field $X(\mathbf{r},t)$ and order parameter fields $\eta(\mathbf{r},t)$, are employed to describe the mole fraction of solute atoms and the discontinuous displacement field of dislocations at position $\mathbf{r}$ and time t. The lattice distortions caused by solute atoms and dislocations generate stress fields, hence, elastic energy. In the present model the lattice distortions are described by ''eigenstrain or stress-free strain.'' If we assume that the variation of stress-free lattice constant a with respect to composition obeys the Vegard's law, then the local eigenstrain caused by compositional inhomogeneity can be written as

$$\epsilon_{ij}^{0}(\mathbf{r},t)=\epsilon^{0}\,\delta X(\mathbf{r},t)\,\delta_{ij}\,, \tag{1}$$

where $\epsilon^{0}=(1/a)(da/dX)$ is the composition expansion coefficient of lattice constant, $\delta X(\mathbf{r},t)=X(\mathbf{r},t)-X_0$ with X_0 being the overall composition of the solid solution, and δ_{ij} is the Kronecker–Delta function. It should be pointed out the assumption of Vegard's law is not necessary in our model.

Most structural defects such as dislocations, grain boundaries, slip bands, and cracks can be described by their corresponding spatially dependent eigenstrains.[30] With such a concept, an arbitrary distribution of structural defects can be introduced to a phase-field model.[19,20] As a consequence, the stress field due to defects as well as compositional and/or structural inhomogeneity can be calculated by the microelasticity theory developed by Khachaturay and Shatalor.[31,32] In order to describe the dislocation dynamics within the framework of a phase-field model, an order-parameter field, $\eta(\mathbf{r},t)$, which represents the magnitude of the discontinuous relative displacements on slip planes in units of Burgers vector $\mathbf{b}=[b(1),b(2),b(3)]$, i.e., $\mathbf{u}_0=\mathbf{b}\,\eta(\mathbf{r},t)$ was introduced.[22] A definition of dislocation eigenstrain is proposed as[29]

$$\epsilon_{ij}^{\mathrm{dis}}(\mathbf{r},t)=\frac{1}{2d_0}[b(i)n(j)+b(j)n(i)]f[\,\eta(\mathbf{r},t)], \tag{2}$$

where $\mathbf{n}=[n(1),n(2),n(3)]$ is the normal direction of the slip plane, d_0 is the spacing of slip planes, and

$$f[\,\eta(\mathbf{r},t)]=\eta(\mathbf{r},t)-\frac{1}{2\pi}\sin[2\pi\eta(\mathbf{r},t)]. \tag{3}$$

The function $f[\,\eta(\mathbf{r},t)]$ has the following two properties: (i) it is exactly equal to $\eta(\mathbf{r},t)$ when $\eta(\mathbf{r},t)$ is an integer; and (ii) its derivatives at integer values of $\eta(\mathbf{r},t)$ are zero. These properties eliminate the dependence of dislocation Burgers vector on the applied stress for dislocation motion and yield correct stress fields for both static and dynamic dislocations.[29] Another important feature of the definition of eigenstrain is that it results in a smaller effective radius of the dislocation core and thus improves the accuracy of the dislocation stress field. In the numerical simulation, if we choose the grid spacing to be about the size of dislocation core (several lattice constants), the calculated elastic stress field is exactly in agreement with the analytical solution except at the two points at the dislocation core where the elastic solution is no longer valid.[29] In addition, since the discontinuous displacement at the dislocation core is described by a smooth function, it implies that the dislocation core is spread out within the glide plane like the Peierls–Nabarro model.[33,34] As a result, unlike the analytical solution, the stresses at dislocation core is no longer singular. The elimination of the singularity not only leads to a stress field which is closer to the real situation but also benefits the numerical stability.

In a single crystal with N slip systems, N-order parameter field variables $\eta_{\alpha\beta}(\mathbf{r},t)$ ($N=\Sigma_{\alpha=1}^{p}m_\alpha$, $\alpha=1,2,...,p$; $\beta=1,2,...,m_\alpha$) are needed to represent the dislocation systems, where p and m_α denote the number of elementary slip planes and elementary Burgers vectors on the related slip plane α. For instance, in a fcc single crystal, there are four slip planes: (111), ($\bar{1}11$), (1$\bar{1}$1), (11$\bar{1}$), and three slip directions on each slip plane, and hence it requires 12 order parameter field variables [$p=4$, and $m_\alpha=3$ ($\alpha=1,2,3,4$)]. Therefore, the eigenstrain for a given dislocation distribution $\eta_{\alpha\beta}(\mathbf{r},t)$ can be written in the Burgers vector $\mathbf{b}_{\alpha\beta}$ and $\mathbf{n}_\alpha$ as

$$\epsilon_{ij}^{\mathrm{dis}}(\mathbf{r},t)=\sum_{\alpha,\beta}\frac{b_{\alpha\beta}(i)n_\alpha(j)+b_{\alpha\beta}(j)n_\alpha(i)}{2d_0}f[\,\eta_{\alpha\beta}(\mathbf{r},t)]$$

$$=\sum_{\alpha,\beta}\epsilon_{ij}^{\mathrm{dis}}(\alpha,\beta)f[\,\eta_{\alpha\beta}(\mathbf{r},t)]. \tag{4}$$

The total eigenstrain associated with compositional inhomogeneity and arbitrary distribution of dislocations is then given by

$$\epsilon_{ij}(\mathbf{r},t)=\epsilon_{ij}^{0}(\mathbf{r},t)+\epsilon_{ij}^{\mathrm{dis}}(\mathbf{r},t). \tag{5}$$

III. THERMODYNAMICS OF A BINARY SYSTEM WITH DISLOCATIONS

The total free energy E in a binary system with dislocations includes (1) the chemical free energy E^{chem} which consists of both the local bulk free energy of a binary solution and the composition gradient energy; (2) elastic energy E^{elast} associated with solutes, defects, and applied stresses; and (3) ''crystalline energy'' which includes the local structural energy and the structural gradient energy. For a perfect dislocation, the crystalline energy is associated with the dislocation core energy.

A. Chemical free energy

In a binary system with a spatial composition distribution $X(\mathbf{r})$, the chemical free energy can be described as the sum of two contributions, i.e., the local bulk free energy and the gradient energy. It reads

$$E^{\text{chem}}=\int_v [(f_0(X)+\kappa(\nabla X)^2]dv, \tag{6}$$

where the first term $f_0(X)$ is the bulk free energy density of a binary solution; the second term is the gradient energy density, and κ is the gradient energy coefficient. For simplicity, we assume regular solution model for $f_0(X)$ which has the form

$$f_0(X)=RT[\varphi X(1-X)+X\ln(X)+(1-X)\ln(1-X)], \tag{7}$$

where R is the ideal gas constant, T is the absolute temperature, and φ is a material constant. For an ideal solution, φ is equal to zero.

B. Elastic energy of the system

The total elastic strain energy can be calculated by (see Refs. 19, 31, and 32 for detail)

$$E^{\text{elast}}=\int_v \frac{1}{2}\lambda_{ijkl}\epsilon_{ij}^{\text{el}}\epsilon_{kl}^{\text{el}}dv, \tag{8}$$

where

$$\epsilon_{ij}^{\text{el}}=\Bigg[\overline{\epsilon}_{ij}+\delta\epsilon_{ij}(\mathbf{r})-\epsilon_{ij}^{0}(\mathbf{r},t)-\sum_{\alpha,\beta}\epsilon_{ij}^{\text{dis}}(\alpha,\beta)f[\eta_{\alpha\beta}(\mathbf{r},t)] - \epsilon_{ij}^{def_0}(\mathbf{r})\Bigg], \tag{9}$$

λ_{ijkl} is the elastic constant tensor, $\overline{\epsilon}_{ij}$ the homogeneous macroscopic strain characterizing the macroscopic shape and volume change, $\delta\epsilon_{ij}(\mathbf{r})$ heterogeneous strains, and $\epsilon_{kl}^{def_0}(\mathbf{r})$ the eigenstrain associated with other defects such as precipitates.

C. "Crystalline energy" associated with dislocations

As a microscopic interpretation, the order parameter $\eta_{\alpha\beta}$ represents the relative displacement between two atomic planes on the slip plane. Imitating the "Peierls potential" in a crystal and the gradient energy in the diffuse-interface theory, Wang *et al.*[22,23] constructed a "crystalline energy" of dislocations

$$E^{\text{cryst}}=\int_v\Bigg[\sum_{\alpha=1}^{p}\sum_{\beta=1}^{m_\alpha}A(\alpha,\beta)\sin^2[\pi\eta_{\alpha\beta}(\mathbf{r},t)] + \frac{\gamma}{2}\sum_{\alpha_1=1}^{p}\sum_{\alpha_2=1}^{p}\Bigg[B_{ijkl}(\alpha_1,\alpha_2) \times\frac{\partial b_i(\alpha_1,\mathbf{r},t)}{\partial r_j}\frac{\partial b_k(\alpha_2,\mathbf{r},t)}{\partial r_l}\Bigg]dv, \tag{10}$$

where γ is a positive constant, $A(\alpha,\beta)$ and $B_{ijkl}(\alpha_1,\alpha_2)$ are material constants that can be fitted to the dislocation core energy and the dislocation core size, and $\mathbf{b}(\alpha,\mathbf{r},t)$ is the total Burgers vector of dislocations at $\mathbf{r}$ on slip plane α

$$\mathbf{b}(\alpha,\mathbf{r},t)=\sum_{\beta=1}^{m_\alpha}\mathbf{b}_{\alpha\beta}\eta_{\alpha\beta}(\mathbf{r},t). \tag{11}$$

In Eq. (10) the first term is the "Peierls potential" (local structural energy), and the second term is the structural gradient energy.

It should be pointed out that the "Peierls potential" does not provide a Peierls stress for the dislocation motion described by the time-dependent Ginzburg–Landau equation, i.e., the Peierls stress is zero for an isolate dislocation in the perfect crystal in the continuum description although the discretizing lattice may provide a pinning force on the dislocation motion.[29]

IV. PHASE FIELD KINETIC EQUATIONS

The temporal evolution of solute composition X is described by the Cahn–Hilliard nonlinear diffusion equation

$$\frac{\partial X(\mathbf{r},t)}{\partial t}=M\nabla^2\frac{\delta E}{\delta X(\mathbf{r},t)}+\xi(\mathbf{r},t), \tag{12}$$

where E is the total free energy of the system, and M is a kinetic coefficient related to the solute diffusion mobility. $\xi(\mathbf{r},t)$ is the noise term. Substituting the total energy into the Cahn–Hilliard Eq. (12) and taking the first variational derivatives with respect to the composition function $X(\mathbf{r},t)$. The composition field kinetic equation is given by

$$\frac{\partial X(\mathbf{r},t)}{\partial t}=M\nabla^2\Bigg\{-\lambda_{ijkl}\epsilon^0\delta_{ij}[\overline{\epsilon}_{kl}+\delta\epsilon_{kl}(\mathbf{r},t)] +\lambda_{ijkl}(\epsilon^0)^2\delta_{ij}\delta_{kl}X(\mathbf{r},t) +\lambda_{ijkl}\epsilon^0\delta_{ij}\Bigg\{\sum_{\alpha\beta}\epsilon_{kl}^{\text{dis}}(\alpha,\beta)f[\eta_{\alpha\beta}(\mathbf{r},t)] +\epsilon_{kl}^{def_0}(\mathbf{r})\Bigg\}+\frac{\partial f_0(X)}{\partial X}-\kappa\nabla^2X(\mathbf{r},t)\Bigg\}+\xi(\mathbf{r},t). \tag{13}$$

The order parameter fields describing the dislocation distribution are nonconserved, and their temporal evolution can be assumed to follow the time-dependent Ginzburg–Landau equations

$$\frac{\partial\eta_{\alpha\beta}(\mathbf{r},t)}{\partial t}=-L\frac{\partial E}{\partial\eta_{\alpha\beta}(\mathbf{r},t)}+\zeta(\alpha,\beta,\mathbf{r},t), \tag{14}$$

where L is the kinetic coefficient characterizing the dislocation mobility, and $\zeta(\alpha,\beta,\mathbf{r},t)$ is the Langevin Gaussian noise term simulating the thermal fluctuations. Equation (14) can be rewritten as

$$\frac{\partial \eta_{\alpha\beta}(\mathbf{r},t)}{\partial t} = L\left\{\lambda_{ijkl}\epsilon_{ij}^{\mathrm{dis}}(\alpha,\beta)\frac{\partial f[\eta_{\alpha\beta}(\mathbf{r},t)]}{\partial \eta_{\alpha\beta}(\mathbf{r},t)} \times\left\{\overline{\epsilon}_{kl}+\delta\epsilon_{kl}(\mathbf{r},t)-\epsilon^0\delta_{kl}X(\mathbf{r},t) -\sum_{\alpha\beta}\epsilon_{kl}^{dis}(\alpha,\beta)f[\eta_{\alpha\beta}(\mathbf{r},t)]-\epsilon_{kl}^{def_0}(\mathbf{r})\right\} -A\pi\sin[2\pi\eta_{\alpha\beta}(\mathbf{r},t)]-\frac{\gamma}{2}\frac{\partial\Phi(\mathbf{r},t)}{\partial\eta_{\alpha\beta}(\mathbf{r},t)}\right\} +\zeta(\alpha,\beta,\mathbf{r},t), \tag{15}$$

where $A=A(\alpha,\beta)$ is assumed to be constant in the simulation for simplicity, and $\Phi(\mathbf{r},t)=\Sigma_{\alpha_1=1}^{p}\Sigma_{\alpha_2=1}^{p}\times[B_{ijkl}(\alpha_1,\alpha_2)\partial b_i(\alpha_1,\mathbf{r},t)/\partial r_j\partial b_k(\alpha_2,\mathbf{r},t)/\partial r_l]$ (see Ref. 23, for detail). To facilitate the computation, we introduce the following dimensionless parameters:

$$r^*=\frac{r}{d_0},\quad d^*=\frac{dx}{d_0},\quad \epsilon_0=\frac{a_0}{d_0},$$

$$\lambda_{ijkl}^*=\frac{\lambda_{ijkl}}{G},\quad \epsilon_{ij}^*=\frac{\epsilon_{ij}}{\epsilon_0},\quad \sigma_{ij}^*=\frac{\sigma_{ij}}{G\epsilon_0},$$

$$A^*=\frac{A}{G\epsilon_0^2},\quad \gamma^*=\frac{\gamma}{2Gd_0^2\epsilon_0^2},\quad t^*=LG\epsilon_0^2t, \tag{16}$$

$$M^*=\frac{M}{Ld_0^2},\quad \kappa^*=\frac{\kappa}{Gd_0^2\epsilon_0^2},$$

$$f_0^*(X)=\frac{f_0(X)}{G\epsilon_0^2},\quad E^{elas*}=\frac{E^{elas}}{G\epsilon_0^2},\quad \chi^*=\frac{RT}{G\epsilon_0^2},$$

where G is the shear modulus, and dx is the grid size of the computational mesh.

V. RESULTS AND DISCUSSION

In the phase-field model formulated above, the dynamic interaction between diffusive solutes and moving dislocations can be obtained by solving the above phase-field kinetic Eqs. (13) and (15). These equations are solved using the semi-implicit spectral method[35] with periodic boundary conditions along $x(r_1)$, $y(r_2)$, and $z(r_3)$ directions. In our simulations the following parameters are fixed: $C_{11}=3.0$, $C_{12}=1.0$, $C_{44}=1.0$, $\varphi=1.5$, $A^*=0.05$, $\gamma^*=0.25$, $\kappa^*=0.05$, $\epsilon^0=0.075$, $\chi^*=0.09$, $\epsilon_0=0.25$, $dt^*=0.2$, $d^*=1.0$, and $d_0=4a_0$ where C_{ij} are dimensionless elastic constants in the Voigt's notation, and a_0 is the lattice constant. We vary the dimensionless parameters M^*, X_0, and $\overline{\sigma}_{31}^*$ to study their effect on dislocation-solute interactions. M^* is the ratio of solute mobility to dislocation mobility. X_0 is the overall composition of the solid solution. $\overline{\sigma}_{31}^*$ is the applied external shear stress. For revealing the basic features of dislocation-solute dynamic interactions, we only consider a single dislocation loop in a two-dimensional problem in the present article although the model is valid for an arbitrary spatial distribution of dislocations in three dimensions. The size of the computational cell is 512×256 corresponding to a crystal of $2048a_0\times1024a_0$. The dislocation loop with a radius $R=80dx$ is introduced into the center of the computational cell by assigning the initial value $\eta=1$ on the grid points inside the dislocation loop on the slip plane and $\eta=0$ outside the loop as shown in Fig. 1. The Burgers vector of the dislocation loop is artificially assumed to be $\mathbf{b}=(100)$ along the x-direction, and its slip plane is $\mathbf{n}=(001)$ plane. We start the simulation with a uniform solute distribution and a dislocation loop under a constant applied strain $\overline{\sigma}_{31}^*$.

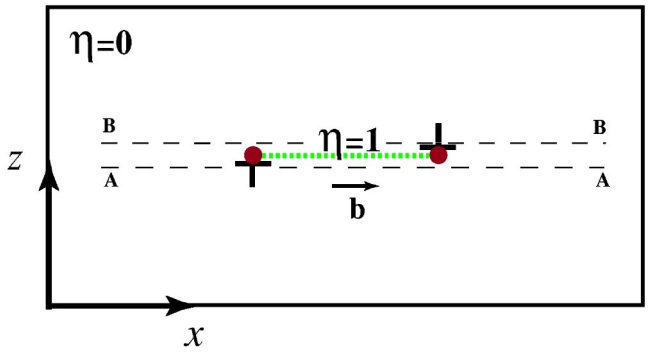

FIG. 1. Schematic illustration of a dislocation loop located at the center of a 2D computational cell.

A. Average velocity of dislocations

To investigate the macroresponses of dislocations to an applied stress, we first study the average velocity of dislocations. Figure 2 presents the average velocity of a dislocation during 1200 simulation steps as a function of M^*, X_0, and $\overline{\sigma}_{31}^*$. It is easy to see from Fig. 2(a) that the average velocity V^* decreases with increasing X_0 for given M^* and $\overline{\sigma}_{31}^*$. The phenomenon reflects the fact that a higher overall solute composition X_0 causes a higher degree of solute segregation near a moving dislocation, hence a larger dragging stress and a lower velocity. Three characteristic velocities of dislocations are observed from Figs. 2(a) and 2(b) for any given X_0 and $\overline{\sigma}_{31}^*$. One of them corresponds to the extreme case of M^* being close to zero. This implies that solute diffusion is very slow compared to dislocation motion. As a result, solute segregation occurs mainly in the dislocation core region where a high driving force exists due to the large stress gradient. The dislocation velocity reaches a maximum value of $V^*=0.16(d_0/t^*)$ at $\overline{\sigma}_{31}^*=0.04$. The maximum value is almost independent of the overall composition X_0, but depends on the magnitude of the applied stress $\overline{\sigma}_{31}^*$ [see Fig. 2(b)].

In order to explain the constant velocity at $M^*=0$, we performed a phase plane analysis.[36] On the slip plane shown in Fig. 1, the evolution Eq. (15) degenerates to a one-dimensional equation

$$\frac{\partial\eta_0}{\partial t^*}=2\gamma^*\frac{\partial\eta_0}{\partial x^{*2}}-A^*\pi\sin(2\pi\eta_0) +2[\overline{\sigma}_{31}^*+\sigma_{31}^*(x^*)]\epsilon_{31}^{\mathrm{dis}*}\frac{\partial f(\eta_0)}{\partial\eta_0} =0, \tag{17}$$

where $x^*=x/d_0$, and $\sigma_{31}^*(x^*)$ is the stress component of the

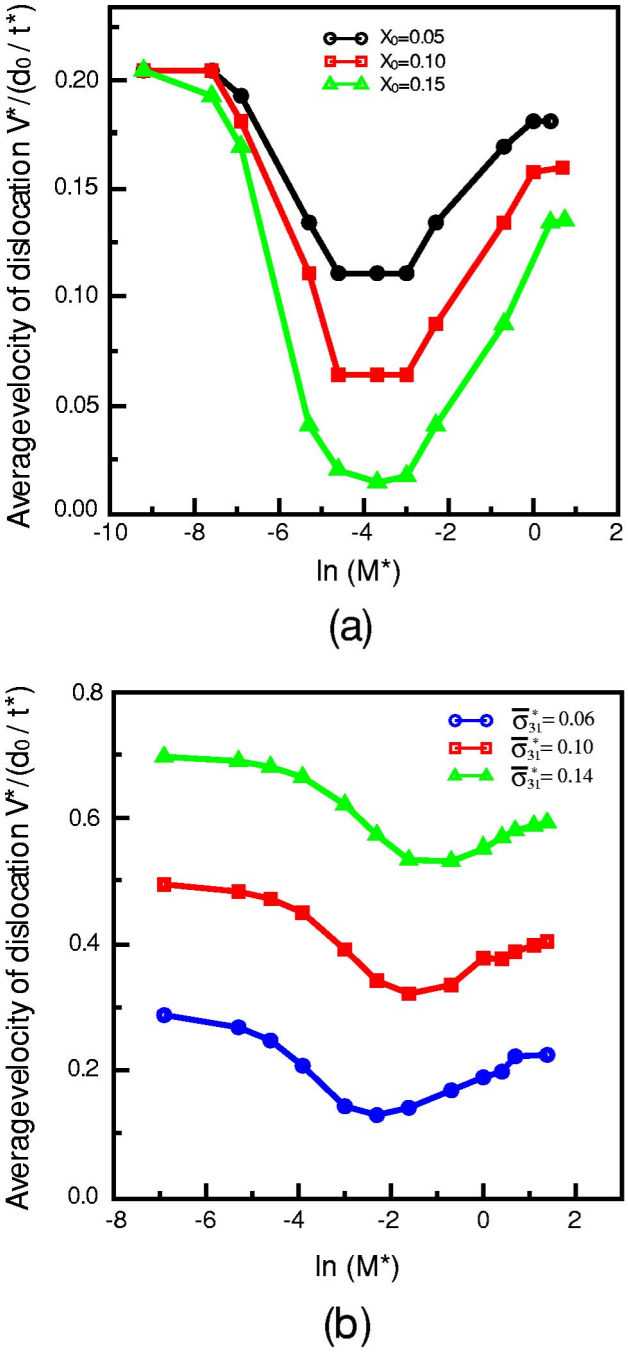

FIG. 2. Average velocity of a dislocation is a function of $M^*=M/Ld_0$, (a) for different overall composition under applied stress $\bar{\sigma}_{31}^*=0.04$; (b) for overall composition $X_0=0.15$ under different applied stresses.

dislocation along the x-direction on the slip plane. We assume that Eq. (17) has a traveling wave solution $\eta_0(x^*)$, and the velocity of the traveling wave, i.e., the dislocation velocity, is V^*. In the moving coordinate system

$$\zeta = x^* - V^* t^* \tag{18}$$

Eq. (17) can be rewritten as

$$2\gamma^* \frac{\partial \eta_0}{\partial \zeta^2} + V^* \frac{\partial \eta_0}{\partial \zeta} - A^* \pi \sin(2\pi\eta_0) + 2[\bar{\sigma}_{31}^* + \sigma_{31}^*(\zeta)]\epsilon_{31}^{\mathrm{dis}*} \frac{\partial f(\eta_0)}{\partial \eta_0} = 0. \tag{19}$$

Multiply both sides with $\eta_0(\zeta)$ and integrate from $(-\infty,\infty)$, we get the velocity V^*

$$V^* = \frac{\int_0^1 2[\bar{\sigma}_{31}^* + \sigma_{31}^*(\zeta)]\epsilon_{31}^{\mathrm{dis}*} \frac{\partial f(\eta_0)}{\partial \eta_0} d\eta_0}{\int_0^1 \eta_0'(\zeta) d\eta_0}. \tag{20}$$

The existence of a traveling wave solution for Eq. (17) depends on the property of the third term in the left-hand side of the equation. It can be proved analytically that the traveling wave solution always exist if $\sigma_{31}^*(x^*)=0$ and with the function (3). Generally speaking, the traveling wave $\eta_0(\zeta)$ depends on the applied stress $\bar{\sigma}_{31}^*$. Therefore, Eq. (20) gives a nonlinear relationship between the dislocation velocity and applied stress. However, our numerical analysis showed that for small applied stress $\bar{\sigma}_{31}^*$, $\eta_0(\zeta)$ is close to the equilibrium profile determined in the absence of applied stress $\bar{\sigma}_{31}^*=0.0$. Hence, a linear relationship between the dislocation velocity V^* and the applied stress $\bar{\sigma}_{31}^*$ exists for small applied stresses. Substituting $\bar{\sigma}_{31}^*=0.04$ and the equilibrium profile $\eta_0(\zeta)$, we got $V^*=0.18(d_0/t^*)$. The velocity $0.18(d_0/t^*)$ is slightly larger than $0.16(d_0/t^*)$ obtained by the simulation. The reduction of the average velocity V^* in the simulation may be due to the dragging force resulted from the solute segregation in the dislocation core, since we observed solute segregation in the dislocation core even when M^* is very small.

The second characteristic velocity of dislocation is associated with the other extreme case where M^* is very large. In this case, V^* increases slowly with increasing M^* for given X_0 and $\bar{\sigma}_{31}^*$. As is known, larger M^* implies that the solute diffuses much faster than the dislocation motion. An equilibrium solute segregation profile around a dislocation is instantaneously established. The average dragging stress exerted on the dislocations by the solutes decreases and approaches to a constant which corresponds to the equilibrium solute segregation. As a result, the dislocation velocity increases and becomes a constant as well. Finally, it is shown that there exists a certain value of M^* that leads to the minimum in dislocation velocity. From the results shown in Fig. 2 it can be found that such a M^* is independent of X_0 but increases with the increase of the applied stress $\bar{\sigma}_{31}^*$. The solute atmosphere and dragging stress at such a critical situation will be analyzed in the following sections.

B. Solute atmosphere

For a given overall solute composition $X_0=0.15$ and applied stress $\bar{\sigma}_{31}^*=0.04$, the profiles of solute atmospheres around the moving dislocation are shown in Figs. 3(a)–3(c) for $M^*=0.0005$, 0.02, and 3.0, respectively. As expected, M^* affects significantly the size, shape, and composition

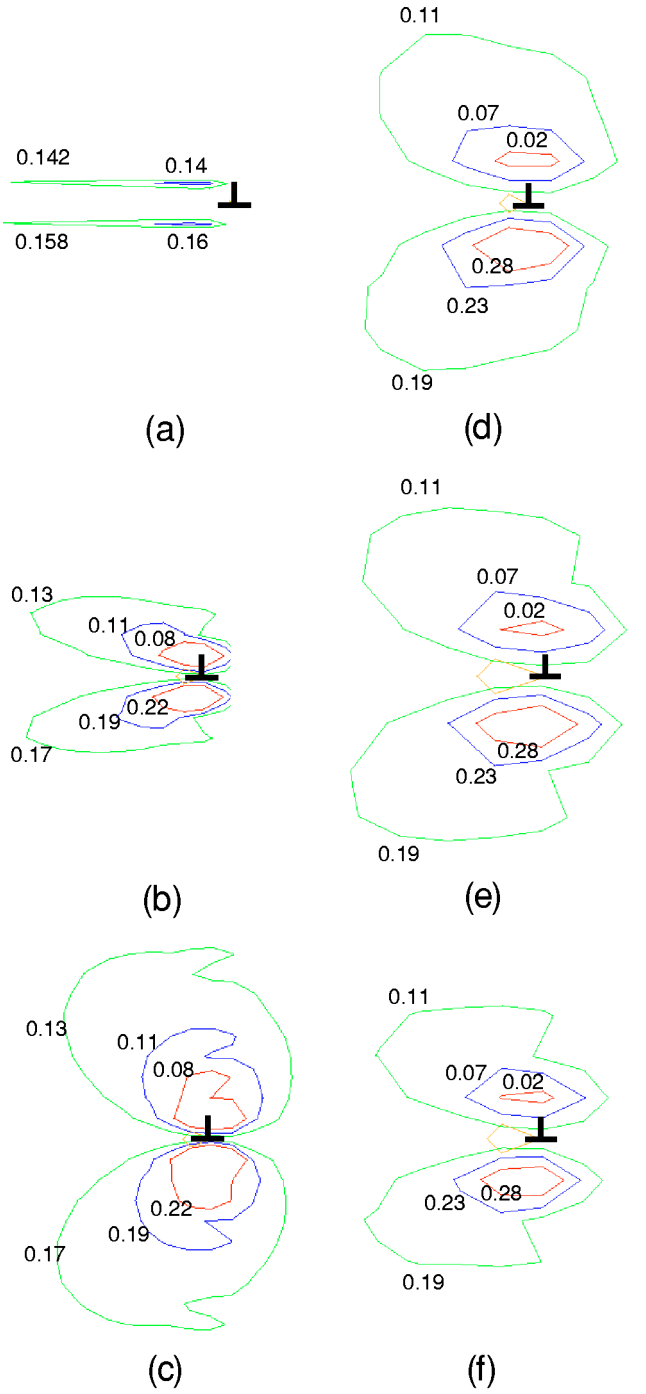

FIG. 3. Solute atmospheres around moving dislocations in a solid solution with overall composition is $X_0=0.15$. (a), (b), and (c) under applied stress $\bar{\sigma}^*_{31}=0.04$ and $M^*=0.0005$, 0.02, and 3.0, respectively; (d), (e), and (f) for $M^*=0.5$ and different applied stresses $\bar{\sigma}^*_{31}=0.06$, 0.1, and 0.14, respectively.

profile of solute atmospheres. More interestingly, we found from Figs. 3(b) and 3(c) that a higher degree of segregation does not always lead to a larger dragging stress. The reason is that the dragging stress is largely affected by the relative position of the dislocation in the solute atmosphere. The obvious change of the dislocation position can be observed in Figs. 3(a)–3(c). In Figs. 3(d)–3(f) we present the profiles of the solute atmosphere at $M^*=0.5$ for different applied stresses. It is seen that the applied stress affect the size of the solute atmosphere. A larger applied stress results in a spatially smaller solute atmosphere.

C. A phenomenon of Portevin–Le Chatelier effect and dynamic dragging stress

Portevin–Le Chatelier effect in solid solution results from the alternating segregation of solutes toward dislocations and the unlocking of the moving dislocation from its solute atmosphere. The Portevin–Le Chatelier effect is characterized by a number of experimental observations such as the upper yield point, serration in the tensile stress versus strain curves, and abnormal yield stress which increases and then decreases as temperature increases in a particular temperature region. As a matter of fact, the average dislocation velocity presented in Sec. IV A exhibits a behavior similar to the macroscopic Portevin–Le Chatelier effect. If we assume that the dislocation mobility is constant, Fig. 2 presents a relationship between the average dislocation velocity and the solute mobility since M^* is the ratio of the solute mobility to the dislocation mobility. For substitutional solutes, its mobility strongly depends on temperature, and increases as temperature increases. Therefore, the x-axes in Fig. 2 can be regarded as temperature. All results in Fig. 2 demonstrate a common tendency, i.e., the average dislocation velocity decreases and then increases as temperature increases. Such a dependence of the dislocation velocity implies that the macroscopic yield stress increases and then decreases with an increase in temperature, i.e., the Portevin–Le Chatelier effect. Of course, for a quantitative simulation of the Portevin–Le Chatelier effect, we need to perform a large scale multidislocation system in three dimensions.

The origin of the Portevin–Le Chatelier effect in the solute solution is the dynamic interaction between solutes and dislocations. In order to examine the dynamic interaction, temporal dislocation velocities and dynamic dragging stress of solute atmosphere are calculated for the cases shown in Figs. 3(a)–3(c) in which the dislocation has the characteristic velocities. The temporal dislocation velocity versus the distance of dislocation motion was plotted in Fig. 4(a). Some features are observed from the results. First, the formation of solute atmosphere slows down the dislocation velocity until it reaches the characteristic average velocity. For example, the velocity dropped from 0.45 to $0.29(d_0/t^*)$ after the dislocation moved about $5-10d_0$ distance for the case of $M^*=0.02$. Since in our simulation we assumed there was no solute segregation around the dislocation at $t^*=0$, the initial velocity should be the same value of $0.45(d_0/t^*)$ for different M^*. Second, the dynamic interaction between the moving dislocation and its solute atmosphere causes a periodic variation of dislocation velocity. It is found that the strength of dynamic dragging corresponding to the amplitude of velocity oscillation is almost independent of M^*. However, the frequency of the dislocation velocity oscillation depends on M^*. Finally, it is interesting to find that the average dislocation velocity decreases as the frequency of the dynamic interaction increases.

In continuum mechanics, the dragging stress of the solute atmosphere is defined as the stress at the dislocation line.

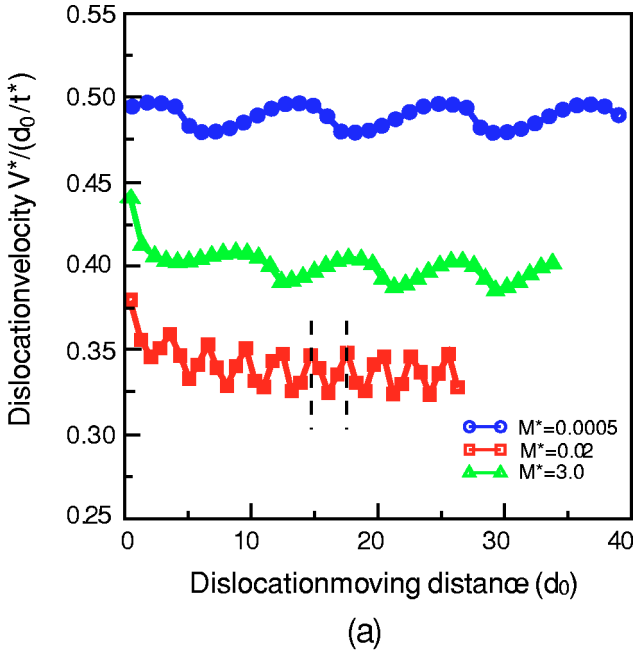

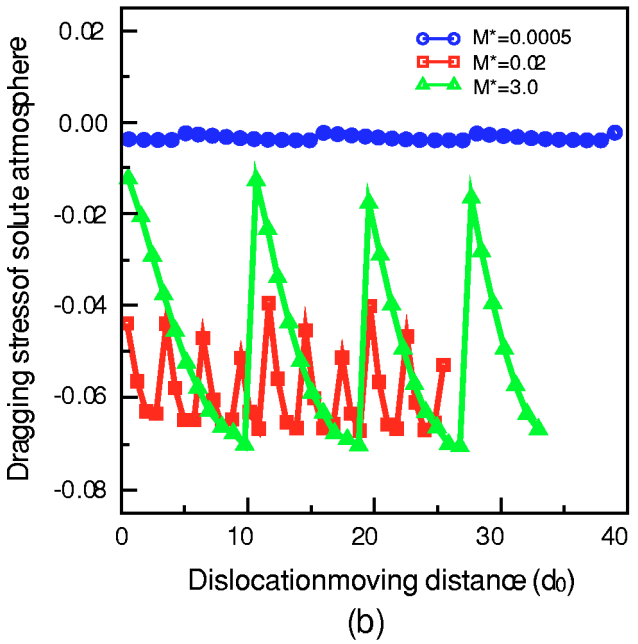

FIG. 4. (a) Dislocation velocity under applied stress $\bar{\sigma}_{31}^{*}=0.1$; (b) dynamic dragging stress of solute atmosphere under applied stress $\bar{\sigma}_{31}^{*}=0.1$.

Figure 4(b) presents the dragging stress of solute atmosphere at dislocation line (η=0.5) during the dislocation motion for the three cases in Fig. 4(a). As expected, the dragging stress changes periodically during the dislocation motion. The change frequency of the dragging stress is consistent with that of the dislocation velocity. In our phase field model, the dislocation core is spread out within the glide plane. Therefore, the stress at the dislocation line (η=0.5) is not exactly the total dragging stress of the solute atmosphere. However, it is found that the average value of the dragging stress during a periodic variation of the dislocation velocity might reflect a total dragging stress.

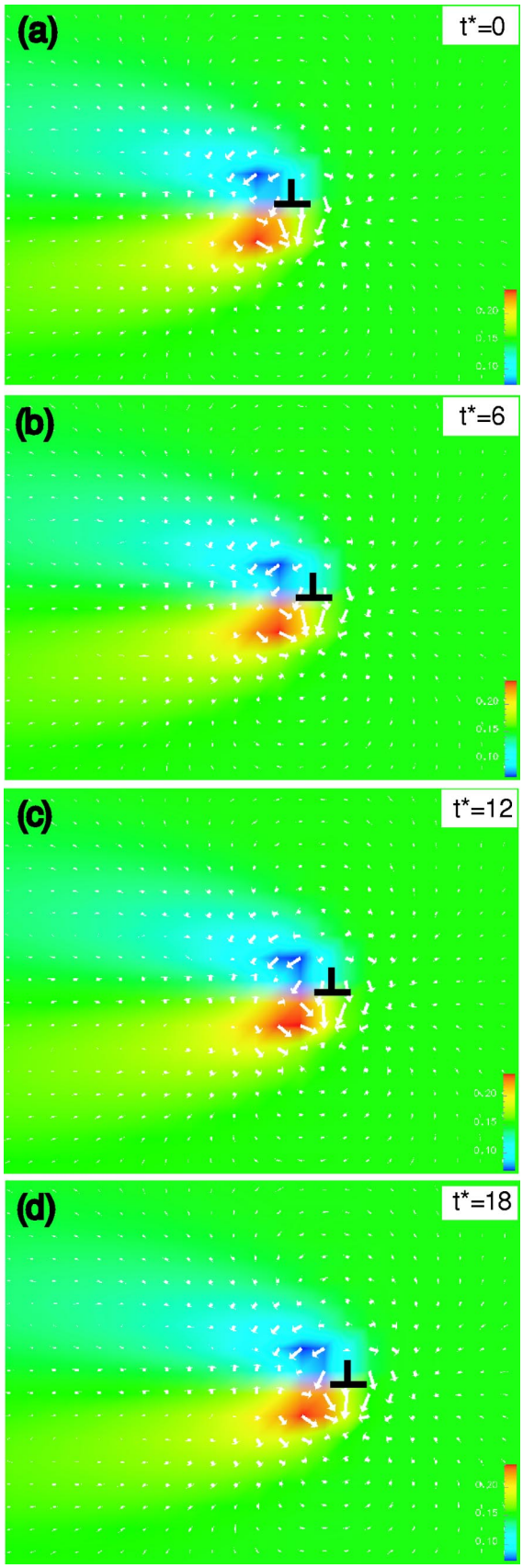

FIG. 5. Dislocation and solute atmosphere move concurrently during the period marked by the dash lines in Fig. 4(a) for the case $M^{*}=0.02$ and applied stress $\bar{\sigma}_{31}^{*}=0.1$.

D. Solute flow around the moving dislocation

Solutes diffuse down along the gradient of total chemical potential which depends on the distribution of solute atoms and elastic interaction energy. A simple model[13] was used to predict the solute flow around a stationary dislocation, which has a constant velocity. In the model, the hydrostaic interaction between a solute atom and an edge dislocation, and the convection of solute atoms to the moving dislocation were considered. However, the effect of the chemical free energy of the solid solution, elastic interactions among solutes, the solute atmosphere around the dislocation on the solute flow were ignored. The phase field model in the present work takes all these effects into account. Figure 5 presents a snapshot of the solute flow during the period marked by the dash lines in Fig. 4(a). The white arrows show the directions of the solute flow, and the length of the arrows denotes the strength of the solute flow. The lighter region below the slip plane and darker regions above the slip plane indicate the solute segregation and depletion regions, respectively. In fact, the solute flow around a moving dislocation can be separated into two parts. The first part is described by the model in Ref. 13. The second part is related to the disappearance of the solute atmosphere left by the moving dislocation. It can be seen that the second part results in the flow lines of the solute atoms that are totally different from that predicted by the analytical calculation.[13]

VI. SUMMARY

The dynamic interactions between moving dislocations and diffusive solutes are studied by a phase-field model. Both the chemical interaction in the solute solution and elastic interactions among solutes and dislocations have been taken into consideration. The simulation results reveal some features of dynamic interactions between a single dislocation and its solute atmosphere. The temporal dragging stress of the solute atmosphere changes periodically, leading to a periodically varied velocity of the dislocation. The average velocity of the dislocation has three characteristic values which depends on the overall composition, the ratio of solute mobility and dislocation mobility, and the applied stress. The dragging stress depends not only on the degree of solute segregation but also the position of the dislocation in the solute atmosphere. Although the simulations are carried out in a solute solution with a single dislocation in two dimensions, the model can be directly applied in a general case of three-dimensional multidislocations. In order to study the PLC effect, however, strain rate, dislocation reactions, and the interaction between moving dislocations and immobile defects have to be incorporated into the model.

ACKNOWLEDGMENTS

The authors are grateful for the financial support from NSF under Grant No. DMR-01-22638 and from ALCOA. The authors also thank H. Weiland and J. Murray for helpful discussions. J.C. acknowledges the support of the Kangung National University, Korea, during his stay at the Pennsylvania State University during 2001–2002.

[1] A. H. Cottrell, Philos. Mag. **44**, 829 (1953).
[2] P. Haasen, in *Dislocations in Solids 4*, edited by F. R. N. Nabarro (North-Holland, New York, 1979).
[3] Jens Lothe and John Price Hirth, *Theory of Dislocations* (McGraw-Hill, New York, 1968).
[4] T. Mohri and T. Suzuki, in *Impurities in Engineering Materials*, edited by Clyde L. Briant (Marcel Dekker, New York, 1999), p. 259.
[5] D. Blavette, E. Cadel, A. Fraczkiewicz, and A. Menand, Science **286**, 2317 (1999).
[6] M. Lebyodkin, L. Dunin-Barkowskii, Y. Brechet, Y. Estrin, and L. P. Kubin, Acta Mater. **48**, 2529 (2000).
[7] J. Friedel, *Electron Microscopy and Strength of Crystals* (Interscience, New York, 1963), p. 605.
[8] R. Labusch, Phys. Status Solidi **41**, 659 (1970).
[9] R. Labusch, Acta Metall. **20**, 917 (1972).
[10] M. Koslowski, A. Cuitino, and M. Ortiz, J. Mech. Phys. Solids **50**, 2507 (2002).
[11] A. H. Cottrell, in *Report of a Conference on Stength of Solids*, edited by N. F. Mott (The Physical Society, London, 1948).
[12] A. H. Cottrell and M. A. Jaswon, Proc. R. Soc. London, Ser. A **199**, 104 (1949).
[13] H. Yoshinaga and S. Morozumi, Philos. Mag. **23**, 1367 (1971).
[14] L. P. Kubin and Y. Estrin, Acta Metall. Mater. **38**, 697 (1990).
[15] M. Lebyodkin, Y. Brechet, Y. Estrin, and L. P. Kubin, Phys. Rev. Lett. **23**, 4758 (1995).
[16] M. Lebyodkin, L. Dunin-Barkowskii, Y. Brechet, Y. Estrin, and L. P. Kubin, Acta Mater. **48**, 2529 (2000).
[17] Y. Wang, D. J. Strolovitz, J. M. Rickman, and R. Lesar, Acta Mater. **48**, 2163 (2000).
[18] D. L. Olmsted, W. A. Curtin, R. J. Clifton, and L. G. Hector, *SES Proceedings of Thr 39th Annual Technical Meeting of the Society of Engineering Science*, Department of Engineering Science and Mechanics (Pennsylvania State University, PA, 2002), pp. 16–17.
[19] S. Y. Hu and L. Q. Chen, Acta Mater. **49**, 463 (2001).
[20] S. Y. Hu and L. Q. Chen, Comput. Mater. Sci. **23**, 270 (2002).
[21] F. C. Larcheand and J. W. Cahn, Acta Metall. **30**, 1835 (1982).
[22] Y. U. Wang, Y. M. Jin, A. M. Cuitino, and A. G. Khachaturyan, Appl. Phys. Lett. **78**, 2324 (2001).
[23] Y. U. Wang, Y. M. Jin, A. M. Cuitino, and A. G. Khachaturyan, Acta Mater. **49**, 1847 (2001).
[24] Y. U. Wang, Y. M. Jin, A. M. Cuitino, and A. G. Khachaturyan, Appl. Phys. Lett. **78**, 2324 (2001).
[25] Y. U. Wang, Y. M. Jin, A. M. Cuitino, and A. G. Khachaturyan, Acta Mater. **49**, 1847 (2001).
[26] J. P. Gunton, M. S. Miguel, and P. S. Sahni, in *Phase Transitions and Critical Phenomena*, Vol. 8, edited by C. Domb and J. L. Lebowitz (Academic, New York, 1983), 267.
[27] C. Chen and Y. Wang, Acta Mater. **51**, 2595 (2003).
[28] D. Rodney, Y. Le Bouar, and A. Finel, Acta Mater. **51**, 17 (2003).
[29] S. Y. Hu, Y. L. Li, Y. X. Zheng, and L. Q. Chen, J. Plasticty **20**, 403 (2004).
[30] T. Mura, *Micromechanics of Defects in Solids* (Kluwer Academic, 1982).
[31] A. G. Khachaturyan and G. A. Shatalov, Sov. Phys. JETP (English transl.) **29**, 557 (1969).
[32] A. G. Khachaturyan, *Theory of Structural Transformations in Solids* (Wiley, New York, 1983).
[33] R. Peierls, Proc. Phys. Soc. London **52**, 34 (1940).
[34] F. R. N. Nabarro, Proc. Phys. Soc. London **59**, 3256 (1947).
[35] L. Q. Chen and J. Shen, Comput. Phys. Commun. **108**, 147 (1998).
[36] Peter Grindrod, *Patterns and Waves* (Clarendon Press, Oxford, 1991), p. 34.